SCIENCE CHINA
Earth Sciences

•RESEARCH PAPER•

January 2020 Vol.63 No.1: 93–107
https://doi.org/10.1007/s11430-019-9376-8

Paleoseismologic record of earthquakes along the Wuzunxiaoer section of the Altyn Tagh fault and its implication for cascade rupture behavior

Zhaode YUAN[1*], Jing LIU-ZENG[1†], You ZHOU[2], Zhigang LI[1,3], Heng WANG[1], Wenqian YAO[1] & Longfei HAN[1]

[1] *State Key Laboratory of Earthquake Dynamics, Institute of Geology, China Earthquake Administration, Beijing 100029, China;*
[2] *Institute of Geomechanics, Chinese Academy of Geological Sciences, Beijing 100081, China;*
[3] *School of Earth Sciences and Engineering, Sun Yat-Sen University, Guangzhou 510275, China*

Received January 14, 2019; revised May 17, 2019; accepted June 10, 2019; published online August 9, 2019

Abstract The Altyn Tagh fault is one of the few great active strike-slip faults in the world. The recurrence characteristics of paleoearthquakes on this fault are still poorly understood due to the lack of paleoseismic records recorded in high-resolution strata. We document a paleoseismic record in a pull-apart basin along the Wuzunxiaoer section of the central Altyn Tagh fault. The high-resolution strata recorded abundant seismic deformations and their sedimentary responses. Four earthquakes are identified based on event evidence in the form of open fissures, thickened strata, angular unconformities, and folds. The occurrence times of the four events were constrained using radiocarbon dating. Event W1 occurred at AD1220–1773, events W2 and W3 occurred between 407 and 215BC, and event W4 occurred slightly earlier at 1608–1462BC, indicating clustered recurrence characteristics. A comparison of the earthquake records along the Wuzunxiaoer section with other records along the Xorkoli section suggests that both sections ruptured during the most recent event.

Keywords Tibet, Altyn Tagh fault, Strike-slip fault, Paleoearthquake, Coseismic offset

Citation: Yuan Z, Liu-Zeng J, Zhou Y, Li Z, Wang H, Yao W, Han L. 2020. Paleoseismologic record of earthquakes along the Wuzunxiaoer section of the Altyn Tagh fault and its implication for cascade rupture behavior. Science China Earth Sciences, 63: 93–107, https://doi.org/10.1007/s11430-019-9376-8

1. Introduction

The Altyn Tagh fault is one of the few great left-lateral active faults in the world and forms the northern boundary of the Tibetan Plateau (Figure 1a). In recent decades, many studies have focused on the fault's initiation time, activity, uplift history, total displacement, deep and shallow structure, and role in the tectonic evolution of Tibet (e.g., Chen et al., 2002; Cheng et al., 2015; Gao et al., 2001; Jiang et al., 2004; Molnar and Tapponnier, 1975; Ritts and Biffi, 2000; Sobel and Arnaud, 1999; Tapponnier et al., 2001; Wang, 1997; Wittlinger et al., 1998; Xiao et al., 2017; Yin et al., 2002; Yue and Liou, 1999; Zhang et al., 2015; Zhao et al., 2006; Chen et al., 2010; Chen et al., 2009; Cui, 2011; Li et al., 2001, 2006, 2007; Liu et al., 2007; Sun et al., 2012; Wu et al., 2012, 2013; Xu et al., 2011). However, studies of the late Quaternary activity of the fault are relatively rare and have mainly focused on the slip rate using geologic and geodetic investigations (Cowgill et al., 2009; Gold et al., 2011; He et al., 2013; Li et al., 2018; Mériaux et al., 2005, 2012; Molnar et al., 1987; Peltzer et al., 1989; Zhang et al., 2007; Wang et al., 2004; Xu et al., 2005). Compared with other famous interplate faults, such as the San Andreas Fault in North America, the North Anatolian Fault in Turkey, the Dead Sea Fault, and the Alpine Fault in New Zealand, the paleoseismology of the

* Corresponding author (email: yzd19862922@163.com)
† Corresponding author (email: liu-zeng@ies.ac.cn)

Altyn Tagh fault has been insufficiently studied (Washburn et al., 2001, 2003; Chinese State Bureau of Seismology, 1992; Xu et al., 2007). In recent years, researchers have performed paleoseismologic studies along the Altyn Tagh fault in an attempt to improve the number of events and their credibility (e.g., Li et al., 2016; Shao et al., 2018; Yuan et al., 2018).

The overall strike of the Altyn Tagh fault is relatively consistent, although several bends divide the fault into different subsections (Ding, 1995). The late Quaternary active trace of the fault has good continuity and is mainly manifested as a single branch. In the middle section of the fault, there are four compressional steps caused by changes in the fault strike between the Cheerchen River and Subei. From west to east, the three most prominent steps are the Akato Tagh, Pingdingshan and Aksay restraining steps (Figure 1b). This type of step plays an important role in controlling the rupture propagation of strong earthquakes, which in turn affects the earthquake magnitude (Biasi and Wesnousky, 2016, 2017; Duan and Oglesby, 2005; Lozos et al., 2011). Although some work has been carried out along these structures (Elliott et al., 2015, 2018; Shao et al., 2018; Washburn et al., 2001, 2003; Yuan et al., 2018), the roles of these steps in the rupture propagation of strong earthquakes are poorly understood. Multiple time-scale slip rates and long sequence paleoseismic data at different locations are required to better understand these processes. In this study, we excavated two paleoseismic trenches along the Wuzunxiaoer section between the Akato Tagh and Pingdingshan steps and correlated the new paleoseismic data with published paleoseismic data along the Xorkoli section to the east of the Pingdingshan step. We then discuss the recurrence characteristics of earthquakes along the central section of the Altyn Tagh fault.

2. Offset landforms along the Wuzunxiaoer section

The ~90-km-long Wuzunxiaoer section of the Altyn Tagh fault, which strikes NE, runs from east of the Akato Tagh bend to north of the Pingdingshan bend. The fault traverses Wuzunxiaoer Lake nearly perpendicular to the shoreline, which has an apparent offset of ~762 m (Figure 2). On the east side of the Akato Tagh (89°37′E–89°43′E), the fault trace is defined by en echelon seismic surface ruptures produced by left-lateral shearing (Molnar et al., 1987; Cowgill et al., 2004). Farther to the east, along the Kulesayi (89°51′45″E–89°52′45″E), the Altyn Tagh fault diverges into several branches in a horsetail pattern. To measure the left-lateral offsets along the section, we used a UAV to take aerial photos of the surface rupture and then processed them with the Agisoft Photoscan software to generate a digital elevation model (DEM) with a resolution of <7 cm (Figure 3a and 3b). Based on the DEM, thirty-nine offsets were obtained by interpreting and restoring offset channels (Figure 3c and 3d),

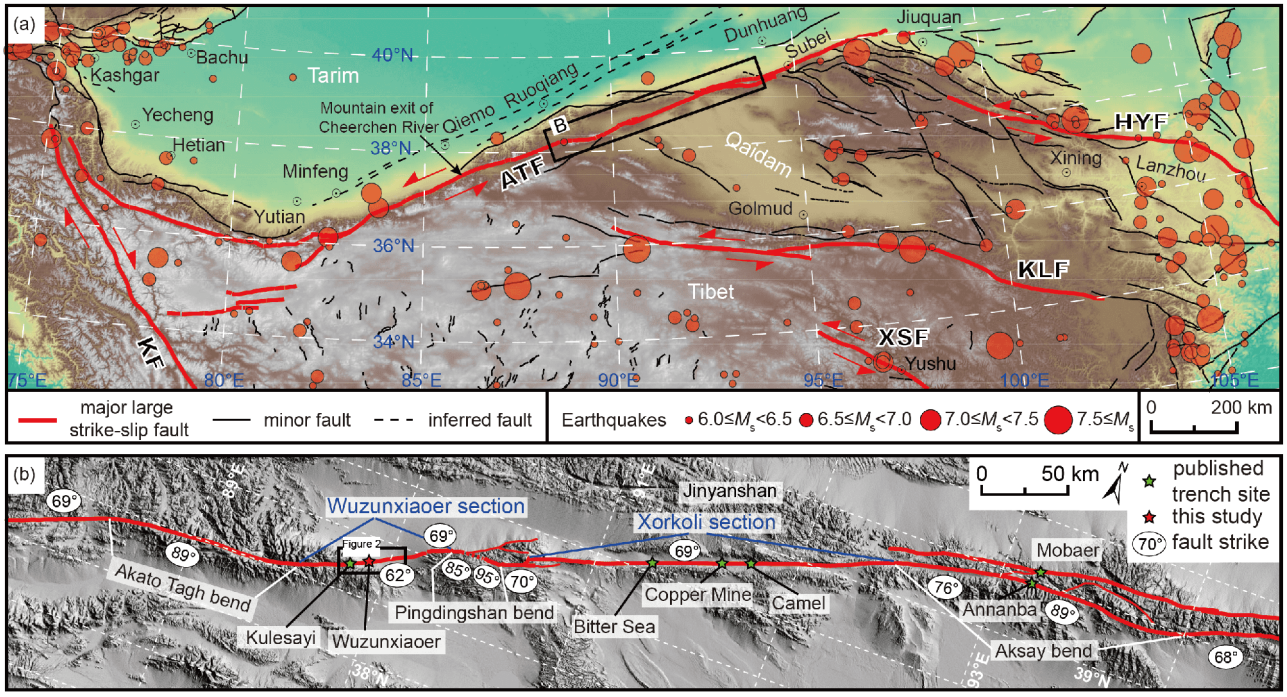

Figure 1 (a) Tectonic setting of northern Tibet showing the locations of faults and historical earthquakes; (b) shaded-relief map of the central section of the ATF and locations of paleoseismic sites. ATF, Altyn Tagh fault; HYF, Haiyuan fault; KLF, Kunlun fault; XSF, Xianshuihe fault; KF, Karakoram fault. All faults are modified from Tapponnier et al. (2001).

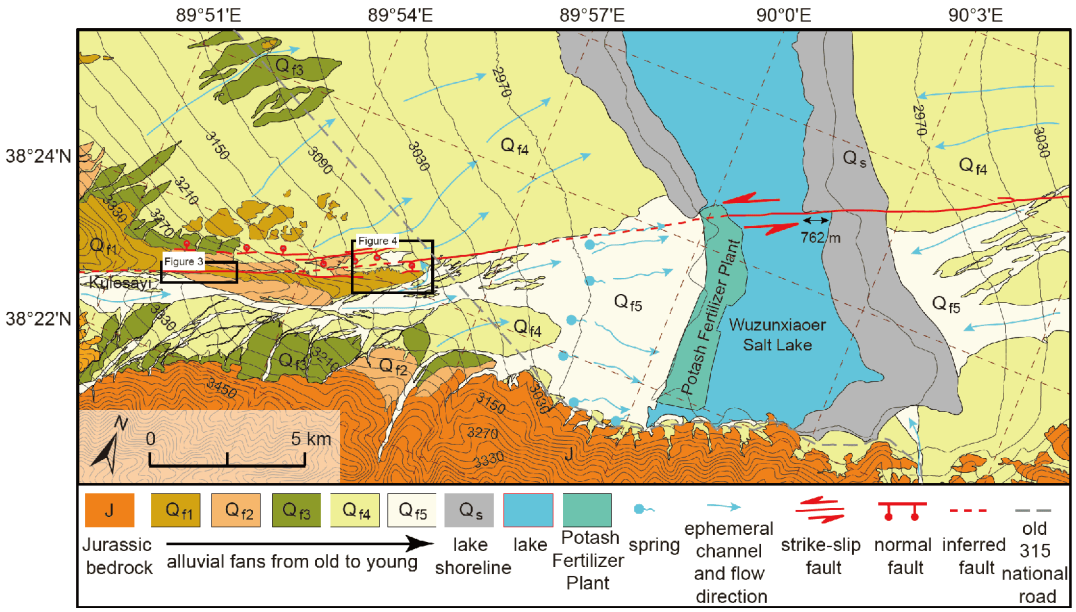

Figure 2 Interpretation of the satellite image of the study area showing a ~762-m sinistral offset of the shoreline and a pull-apart basin on west side of the salt lake. The actual offset of the shoreline is greatly affected by the fault kinematics. Because the ATF is dominated by strike-slip movement and has both thrust and normal faults, ~762 m is the apparent horizontal displacement. The southwestern shoreline of the salt lake has been modified by a potash plant, which results in a lack of an offset shoreline. The background image is from Google Earth.

showing that the coseismic offset of the most recent earthquake was ~6.6 m (Figure 3e). In addition, the 762 m of sinistral displacement indicates that the shoreline has been faulted at least one hundred times, and the latest seismic surface rupture is still clearly preserved in the shallow sediments of the lake.

3. Paleoseismology

3.1 Site description

Based on the principles of site selection for paleoseismic trenching (Liu et al., 2007; Ran et al., 2012; Yuan et al., 2016), two large trenches were excavated in a relatively flat playa in a small pull-apart basin on the west side of Wuzunxiaoer Lake (Figure 4). The basin is located on the west side of the old 315 National Road, where offset landforms have been identified by several scholars (Cowgill et al., 2004; Molnar et al., 1987; Washburn et al., 2001). A series of normal fault scarps with vertical offsets of 2–10 m is located on the northwest side of the basin, and an ancient landslide is located on its southeast side, which may be related to faulting. The Altyn Tagh fault strikes NE62° and passes through the south-central part of the basin. To the east of the playa, the ~20-m-wide earthquake surface rupture zone is located on the alluvial fan (Figure 5). The surface ruptures on the playa and the western alluvial fan have been entirely buried by the debris flow, but the distribution of plants on the playa is consistent with the fault strike, and they are located along the strike of the surface rupture zone, indicating the location of the buried fault traces.

The sediment in the playa, which was shed from peripheral alluvial fans, can be divided into two types, a proximal source and a distal source. The proximal source sediment is mainly pinkish-gray silty sand to clay transported from alluvial fans to the southeast, northwest and southwest of the basin; the distal source sediment comes from the ranges on the southwest side of the basin. The alluvial fan from the bedrock ranges extends to the southeast side of the pull-apart basin and is diverted to the west due to the low-lying terrain of the basin. Some deposits are transported to the basin interior, and fine clastic sediments are deposited in the playa (Figures 4 and 5). Because the bedrock is mainly early-middle Paleoproterozoic to Neoarchean greenish-gray to light gray coarse-grained feldspathic sandstone, conglomerate, and gray to light-gray gneiss and marble, the distal source debris is mainly gray, grayish-green fine sand to clay. Due to the low topography of the basin center, sediments from different sources are continuously deposited in the playa, forming pinkish-gray and greenish-gray rhythmic layering. Moreover, the debris has a high deposition rate and can quickly bury and preserve seismic surface ruptures. This kind of site with a high deposition rate and high-resolution stratigraphy is an ideal trenching site for paleoseismology.

3.2 Strata

Two large trenches, T4 and T5, were excavated across the fault zone in the southern part of the basin. Trench T5 was excavated first. It was 40 m long, 3–4 m wide, and 4.5 m

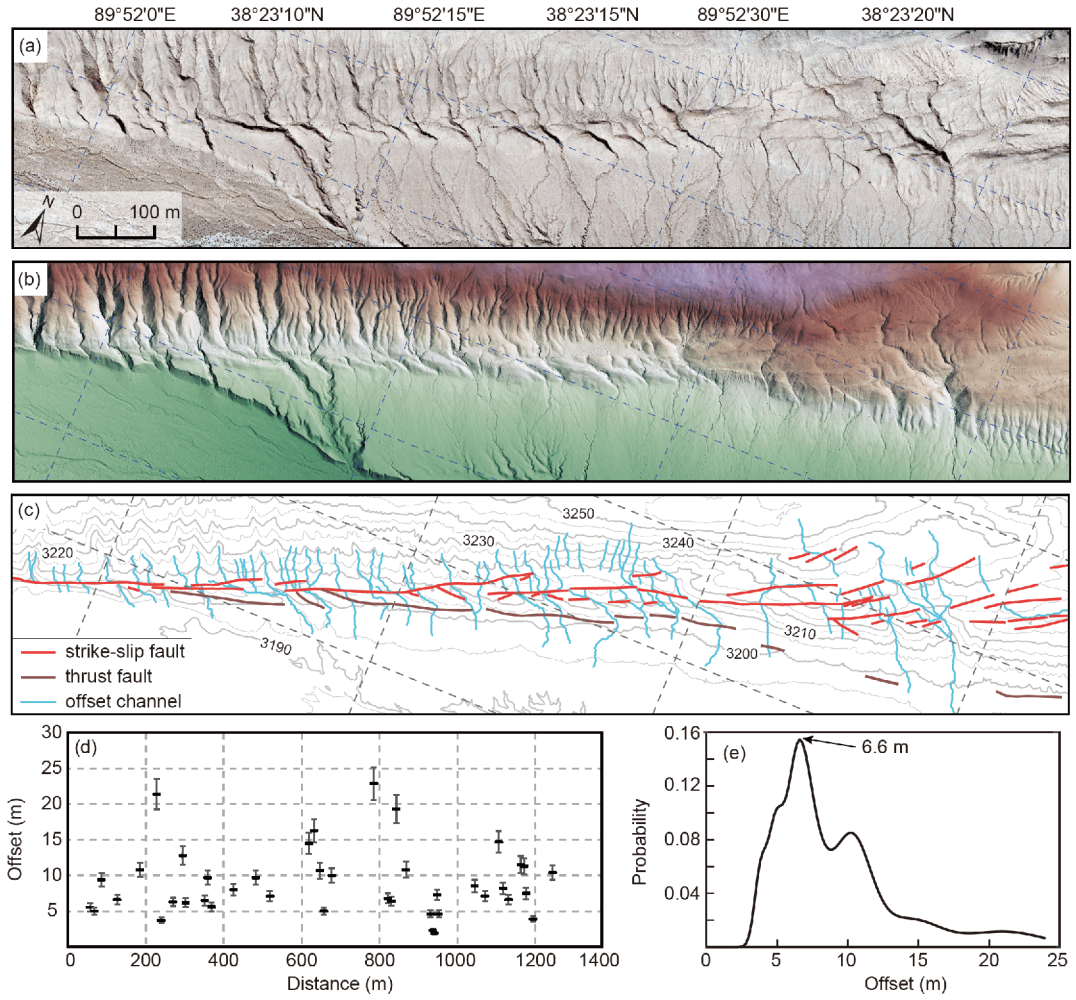

Figure 3 Offset landforms on the west side of the Wuzunxiaoer site and statistics of the channel offset measurements. (a) Mosaic of UAV aerial orthographic images; (b) digital elevation model (DEM); (c) interpretation of channels and faults; (d) plot of offset channels, in which the error is 10% of the offset; (e) probability density diagram of channel offsets.

deep. The strata in the trench are mainly composed of pinkish-gray silt to clay with few rhythmic and traceable strata and three layers of greenish-gray silty sand to clay. These strata characteristics, in which it is difficult to accurately define event horizons, are related to the range of the distal-sourced debris coming from the bedrock mountainous area on the southwest side of the trench. To obtain higher-resolution stratigraphy, we excavated another trench (T4) ~100 m east of T5 and closer to the edge of the alluvial fan. T4 was 28 m long and similar in width and depth to T5. The high-resolution alternating strata in T4 are composed of greenish-gray and pinkish-gray silty sand to clay (Figure 6a and 6b), which fully reflect the characteristics of proximal-source and distal-source interaction. A total of twenty-nine stratigraphic units are identified in T4. The greenish-gray strata can be further subdivided into multiple sets of sub-stratigraphic layers (Figure 7). In addition, the strata in T4 can be traced continually on both walls (Figure 6c and 6d). Thus, the event horizons in T4 can be accurately defined based on the high-resolution and continuous strata.

3.3 Evidence for earthquakes

After detailed mapping of the strata and their structural deformations, four events were recognized primarily by open fissures, folds, angular unconformities, growth strata and vertical offsets. A summary of the surface rupture evidence identified in the two trenches is provided below (Figure 6c, 6d and Figure 8).

(1) Event W1. The most recent ground-rupturing earthquake, event W1, is the most strongly expressed event in the trenches, and it occurred during deposition of unit 50. On the northeast wall of T4 at meters 12 through 13 (all locations are horizontal distances in meters from left to right on the trench wall), the faulting produced a fissure that is overlain by a significantly thickened unit 50. In this exposure, units 120 and 110 warp down into fault zone. At meter 16, units 110 and older are offset by a thrust fault and overlapped by the thickened unit 50. On the hanging wall, unit 110 was partly eroded during the deposition of unit 50. The most impressive feature that formed during event W1 is a thrust fault exposed

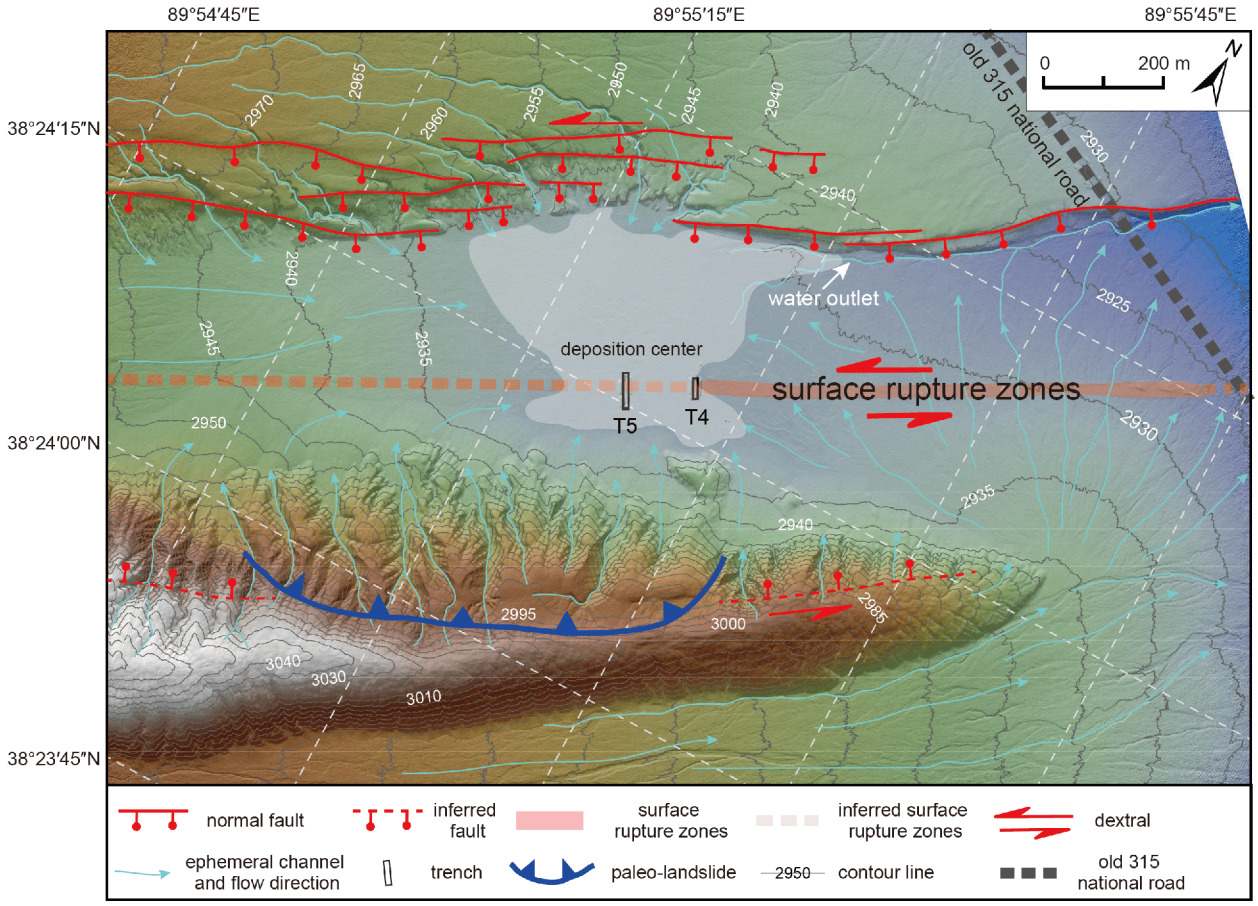

Figure 4 Tectonic geomorphologic map of the pull-apart basin showing the drainage environment, fault traces and trench location superimposed on the digital elevation model (DEM).

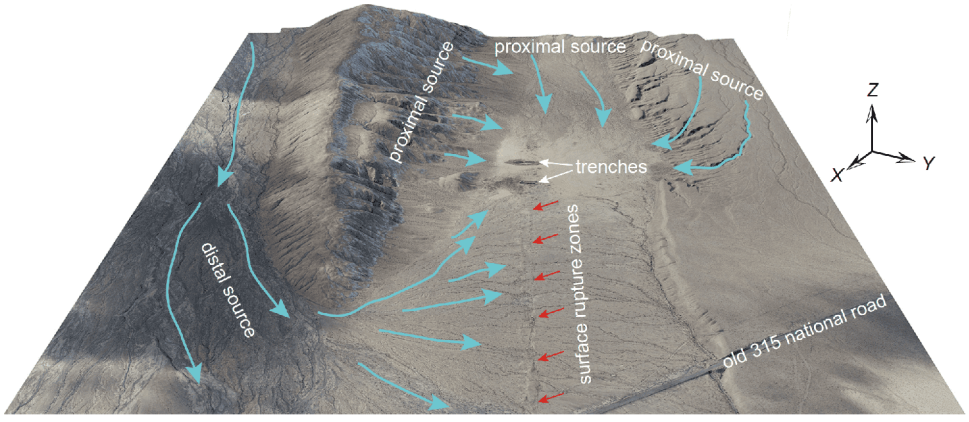

Figure 5 Three-dimensional view of the pull-apart basin showing two debris sources.

on the northeast wall of T4 at meters 21 through 24. Faults clearly cut units 110 and older, which are also folded on the northwest side of the fault zone. The strata in the core of the fold were eroded and lack the overlying unit 50, the thickness of which changes significantly on both sides of the fault zone and forms an angular unconformity with units 110 and 120.

At meter 2 on the southwest wall of T4, faults cut up through the middle of unit 50, generating a fissure that is filled with blocks derived from units 110 and older and is capped by the overlying unit 50, which thickens towards the southeast. At meter 8 in T4SW, a 40-cm-wide fissure with no visible fault below it ruptures up through the lower part of unit 50 and is overlain by the thickened unit 50. Farther to the southeast at meter 10, evidence of the event is very clear as faults rupture up to the lower part of unit 50 and are overlain by the upper part, which thickens into the fault zone. At

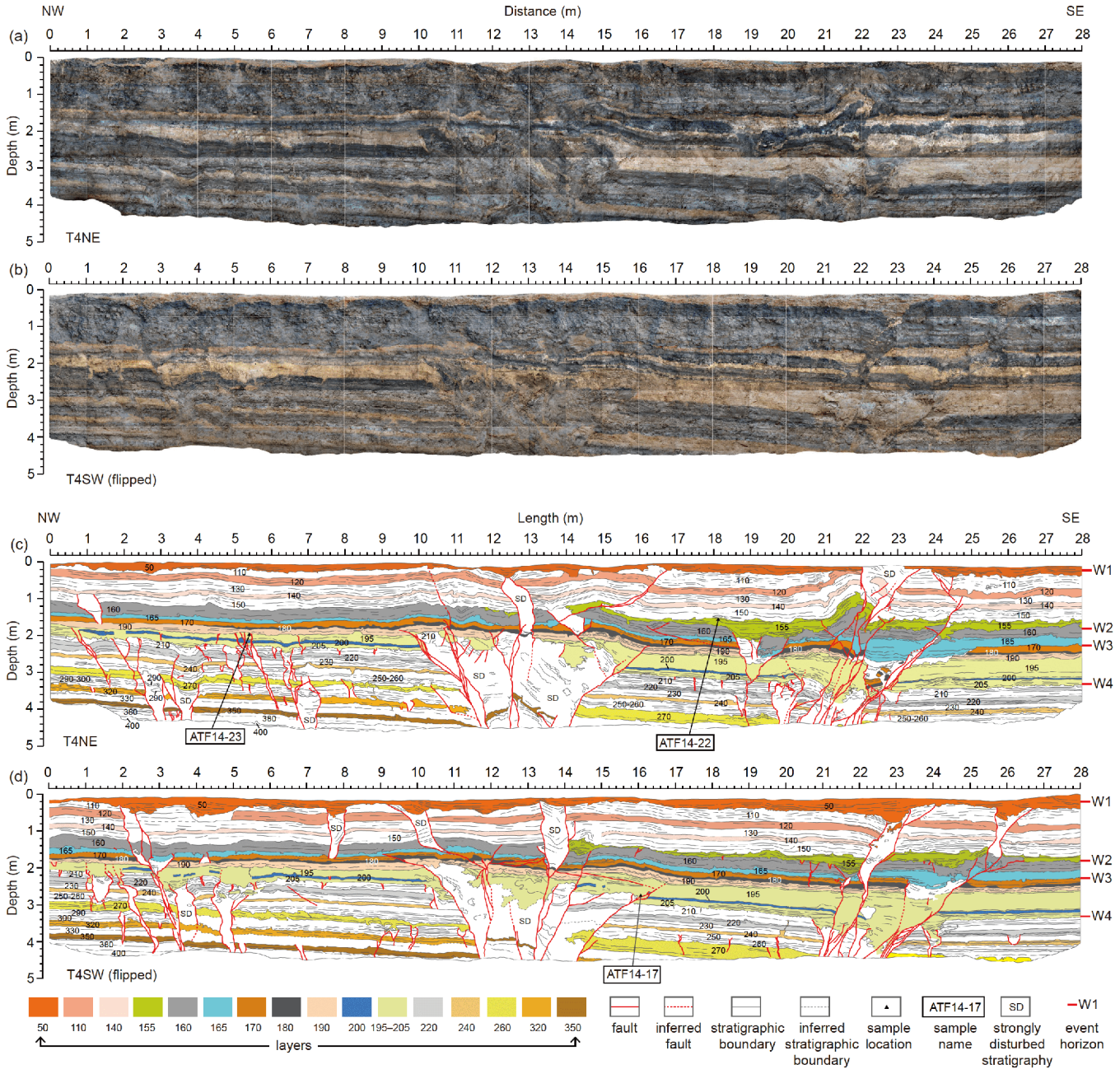

Figure 6 (a)–(b) Photomosaics of the two walls of T4 and (c)–(d) their trench logs at the Wuzunxiaoer site.

meters 13 through 14 in T4SW, units 110 and below are cut by faults that produced a 60-cm-wide fissure. At meters 22–27, two fissures extend through the lower part of unit 50 and are filled with units 50 and older, which are overlain by unit 50, which thickens into the depressions. The strata on both sides of the northwest fissure were vertically offset by ~20 cm.

Event W1 is well-documented in trench T5, and its evidence is clear and significant for identifying the event horizon because unit 50 is ~50 cm thick, significantly thicker than in T4. The area of trench T5 is dominated by the deposition of pinkish-yellow silty sand from the proximal source, while the gray and black sand from the distal source is thin, and some units are even missing. Figure 8 shows that faults clearly cut to the middle of unit 50, forming an angular unconformity between units 50-1 and 50-2. The dating samples defining event W1 were collected in T5 (Figure 8a).

In summary, event W1 occurred during the deposition of layer 50 and has strong credibility due to the large amounts of evidence.

(2) Event W2. The penultimate earthquake (event W2) occurred when unit 160 was at the ground surface. Evidence for event W2 is clear on both walls of T4. A distinct 2-m-wide fissure is located at meters 18–20 in T4NE (Figure 9a).

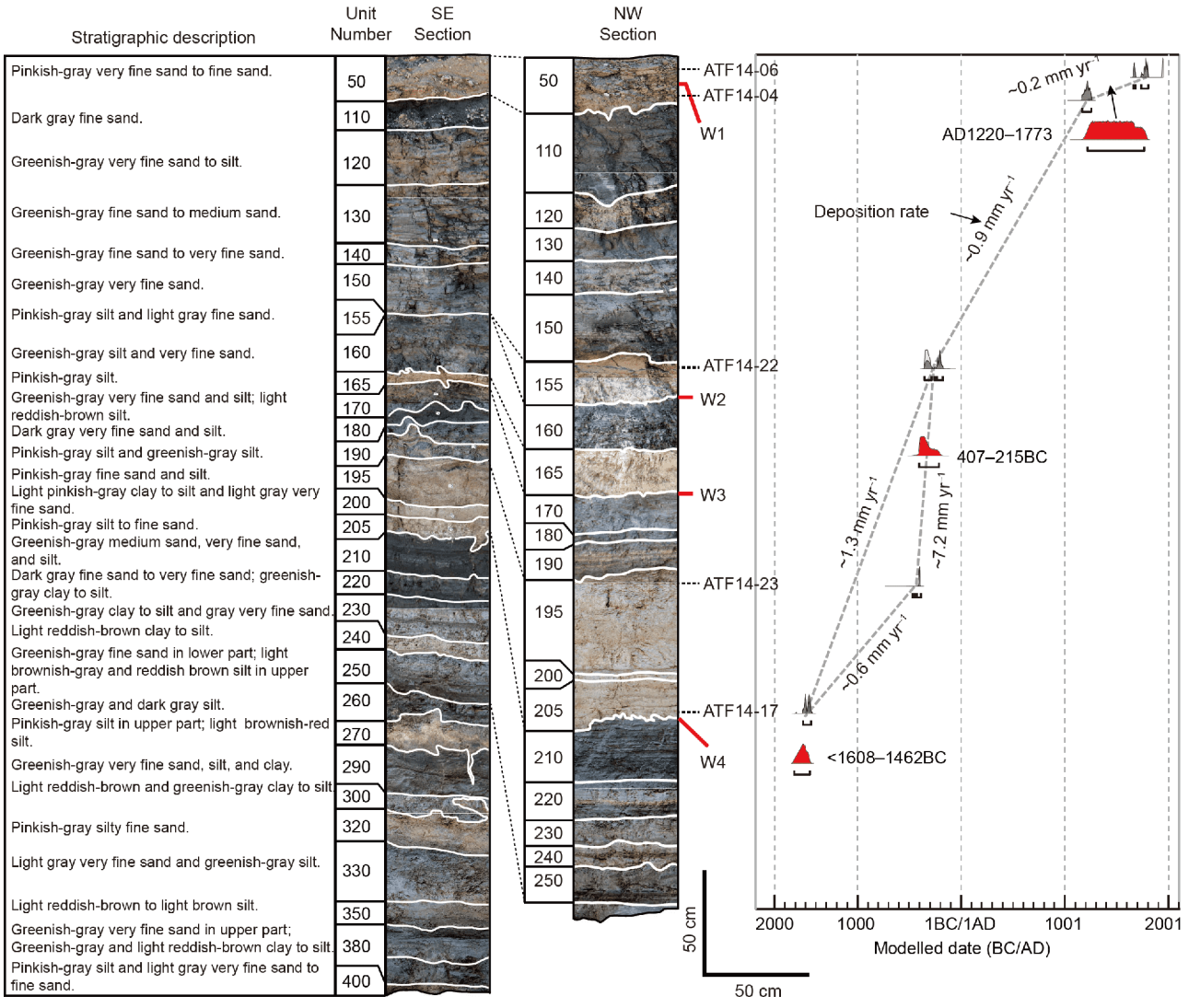

Figure 7 Stratigraphic column, simplified description of strata, and probability density functions (PDFs) for event ages at the Wuzunxiaoer site showing unit thicknesses, unit numbers and stratigraphic locations of radiocarbon samples. The radiocarbon ages were calibrated and statistically analyzed using OxCal 4.3.1 and the atmospheric data from Reimer et al. (2013).

The fissure disrupts units 160 and older, is filled by blocks of units 200–160, and is capped by unit 155, which thickens into the depression. A secondary fault strand on the south side of the fissure cuts to the top of unit 160. At meters 20–22 on the opposite wall (T4SW), faults ruptured through unit 160, producing a fissure that is filled by faulted strata and covered by unit 155, whereas the southeast side of the fissure was faulted by a more recent earthquake. On the northwest side of this exposure, three minor fissures ruptured up through unit 160. At meters 24–25 in T4SW, faults offset units 160 and below, and they are overlain by unit 155, which thickens into the fault zone. The faulting is also overprinted by a younger event. At meter 26.5, the upper part of unit 160 is doubled in thickness by thrust faulting and is overlain by unit 155, which thins dramatically onto the fault scarp. Near meter 15, units 160 and older are cut by a fault and capped by the thickened unit 155.

(3) Event W3. The third earthquake back (event W3) occurred when unit 170 was at the ground surface. The most compelling evidence of event W3 is a large fissure exposed on the northeast wall of T4 in meters 22 through 25 (Figure 9b). This fissure, which is ~3 m wide, clearly cuts units 180 and older and is filled with fragmented blocks derived from units 190 through 170, and it is capped by the thickened unit 165, indicating that the earthquake occurred while unit 170 was at the ground surface. Both sides of the fissure were offset by a younger event. Likewise, on the opposite wall (T4SW), faults displaced units 170 and older, and they were subsequently capped by unit 165, which thickens into the depression.

(4) Event W4. The fourth earthquake (event W4) occurred shortly after unit 210 was deposited. In T4NE, near meter 20,

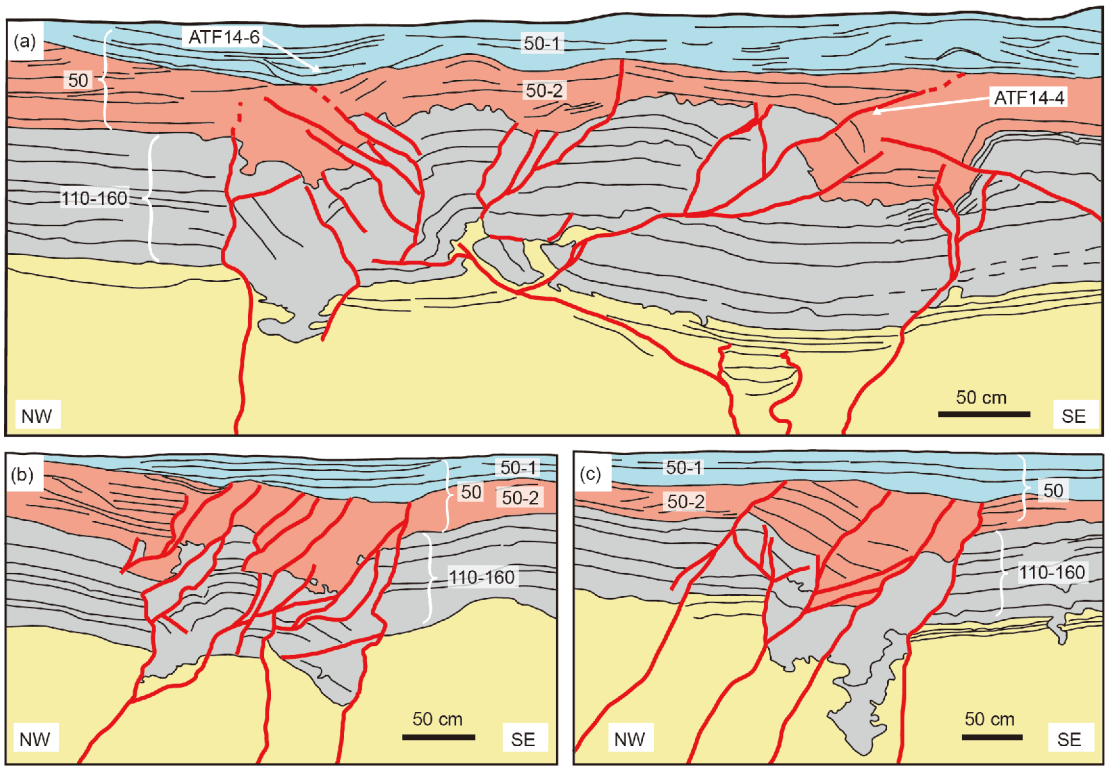

Figure 8 Typical evidence for event W1 in trench T5.

secondary faults offset units 210 and below and are capped by the less-deformed units 205 and 200. At meter 23 in T4NE, a rootless fault cuts unit 210, producing a fissure. One of the most compelling observations is that units 210 and older were folded near meter 3.5 in T4NE, where the overlying unit 205 thickens into the depression, indicating that the earthquake occurred during the early deposition of unit 205 or after the deposition of unit 210. In addition, several minor fissures are located on both sides of the fold, which may be related to the folding.

On the opposite wall (T4SW) at meter 3.8, faults cut to the top of unit 210 and are capped by a significantly thickened unit 205, which was subsequently faulted by event W1. One of the most credible pieces of evidence for this event is at meters 21 and 24 in T4SW, where faults cut to the surface of unit 210, producing fissures filled with greenish-gray and pinkish-yellow sediments and were overlain by unit 205, which thickens into the depressions (Figure 9c). The two fissures appeared to have originally been a single structure before being damaged by a later earthquake. One indication of this is that the overlying unit 205 contains similar sand lenses, both of which were displaced by the younger event.

In conclusion, because the folds, fissure fills and growth strata are strong event indicators, event W4 has high credibility.

(5) Other possible earthquakes in the Wuzunxiaoer trench. At meter 1 in T4NE, the rootless faults cut the upper part of unit 195. A fault near meter 20 in T4NE appears to offset layers to the top of unit 195. However, it is difficult to accurately determine the upper limit due to the poor bedding in the upper part of unit 195. At meter 21, the lower part of unit 195 and the older strata are warped down towards to southeast and are overlapped by less deformed units 190 and the upper part of unit 195. Because the SE side of the exposure is close to the fault zone, the fold deformation may also be related to a later earthquake. At meters 4.6–7 in T4NE and meters 1–5 on the opposite wall, several small fissures terminate at the top of unit 195 and are filled with overlying greenish-gray sediments. Although these fractures may be connected to deeper faults, they may also be mud cracks.

At meter 4 in T4SW, unit 200 shows slight folding deformation, but it is not continuous. In addition, an angular unconformity between unit 190 and the underlying strongly deformed strata can be observed at meters 10 through 16 on both walls in T4, indicating that an earthquake occurred before the deposition of unit 190. However, it is difficult to distinguish the latest underlying strata because the strata are in the main fault zone and have been so strongly deformed that the stratigraphic sequence and sedimentary features cannot be accurately identified. One possibility is that the event horizon is units 195–205, which form an angular unconformity with the overlying unit 190 at meter 11.5 in T4SW. The other possibility is that the event horizon is unit

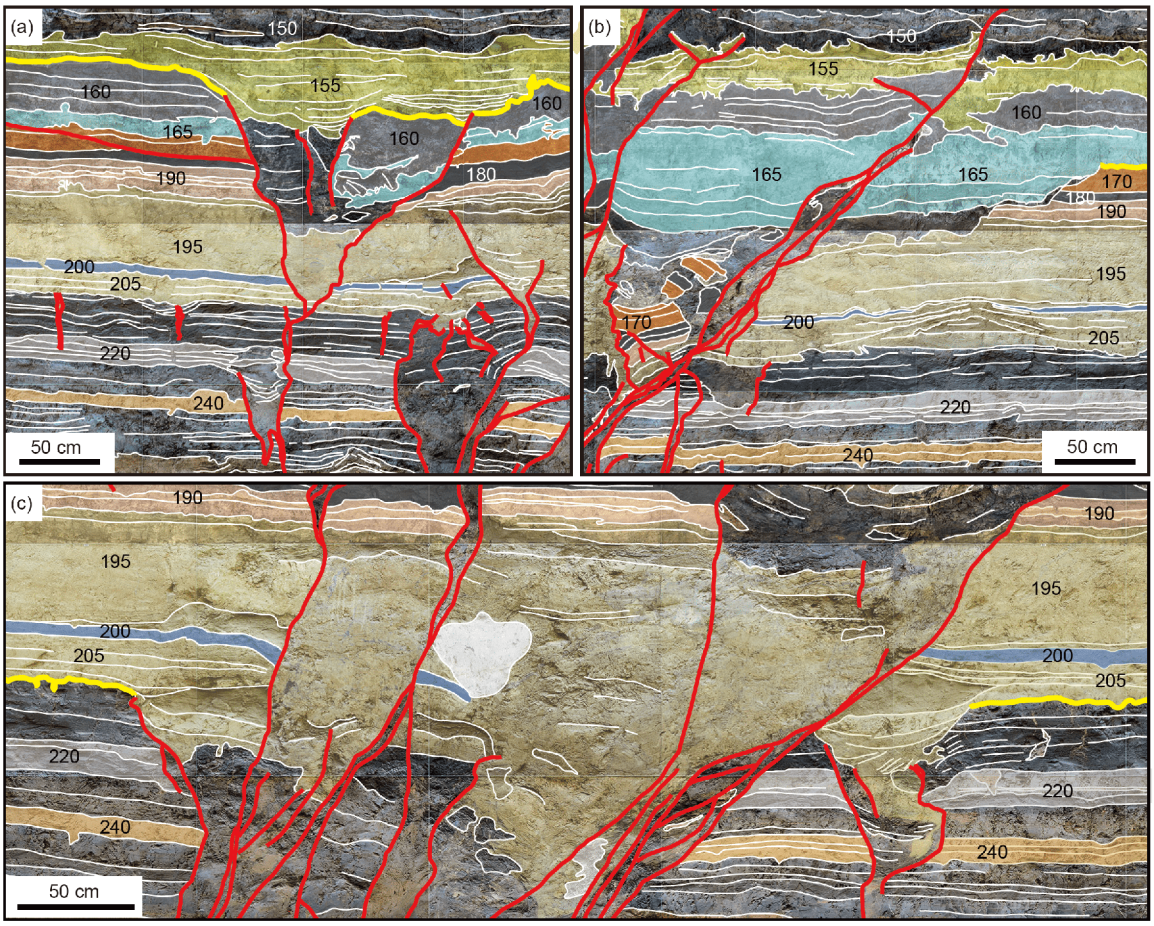

Figure 9 Typical evidence for events W2, W3 and W4 in T4. The bold yellow lines represent event horizons.

210. Most of the underlying units (195–205) are in conformable contact with the overlying unit 190 but have a suspected unconformable contact with the older unit 210. Thus, the earthquake may be event W4. In summary, an event may be preserved in the middle and upper parts of unit 195. However, due to the poor layering of unit 195, the weak continuity of unit 200, and weak indicators such as minor fissures, upward termination of faults and slight folding, the reliability of this earthquake is relatively low.

Faults cut the lower part of unit 260 at meters 2.4–3 in T4NE, producing a fissure filled with blocks of unit 290. Moreover, units 260 and older are strongly disturbed, so it is impossible to distinguish the specific unit. At meter 8 on the same wall, a rootless fault disappears in unit 260. Farther to the southeast at meter 10.3, faults cut to the middle of unit 260. Nearby liquefaction can be observed in unit 270, which affects the central part of unit 260. In summary, an earthquake might have occurred during the deposition of unit 260. However, the thickness of the overlying strata after the earthquake does not change, and there does not appear to be an angular unconformity. Moreover, some deformation was caused by rootless faults. Therefore, the deformation may be secondary deformation caused by more recent earthquakes, so the reliability of this event is low.

At meter 9 in T4SW, there are stratigraphic disturbances in the lower part of unit 270 and unit 290, which may have been caused by an earthquake or freeze-thaw processes. Moreover, minor rootless faults at meters 10 and 11 cut to the base of unit 270, producing two small fissures. The strata on both sides of the fissures do not show obvious vertical offsets. Therefore, an earthquake with low reliability might have occurred during the early deposition of unit 270.

3.4 ^{14}C dating and paleoearthquake ages

In the two trenches, only a small amount of animal dung was found in units 205 and above, and no suitable carbon dating materials were found in the older strata. Five samples were dated at the Keck Carbon Cycle Accelerator Mass Spectrometry Facility at the University of California, Irvine. All of the dating results were calibrated and modeled using the online program OxCal v4.3 (Ramsey and Lee, 2013; Reimer et al., 2013) with 95% confidence intervals (Table 1). Finally, the ages for the paleoearthquakes were modeled accounting

for radiocarbon calibration and stratigraphic constraints (Figure 7). The event horizon of paleoearthquake W1 is in the middle of unit 50. Two radiocarbon samples above and below the horizon provide bounding ages for the paleoearthquake of AD1220–1773. The dates of events W2 and W3 are limited to 407–215BC due to the lack of samples available to constrain their individual dates. The event horizon for W4 is the top of unit 210. Because only one dating sample, ATF14-17, was collected near the base of the overlying unit 205, ~10 cm from the top of unit 210, the date of event W4 should be close to the initial deposition time of the sampling layer, 1608–1462BC. However, sample ATF14-17 was located near the fault zone, which introduces some uncertainty in defining the sample location.

4. Discussion

4.1 Completeness of the Wuzunxiaoer record

Before correlating the events between sites along strike and discussing the recurrence behavior, it is important to evaluate the completeness of the paleoseismic record at each site in terms of the possibility of overestimating or underestimating the number of paleoseismic events. Evaluating the reliability of a paleoearthquake is based on a combination of the quality and frequency of indicators at a particular horizon (Scharer et al., 2007). We used the method of Scharer et al. (2007) to perform a statistical analysis of the earthquake evidence revealed in the trenches. First, each event indicator is assigned a rank indicating the quality of the evidence on a scale of 1 to 4. For example, a rank of 4 (strong) indicates that the morphologic and sedimentologic features could only have been caused by earthquake-induced ground deformation; a rank of 3 (fair) indicates that an earthquake likely formed the features or that it is difficult to confirm the event horizon. A rank of 2 (moderate) indicates that an earthquake possibly caused the features, and a rank of 1 (weak) indicates that an earthquake likely did not cause the features. According to these scoring standards, we evaluated and ranked all of the earthquake indicators exposed in the two trenches. The data set of the suspected event indicators is summarized in Figure 10, which shows that four highly credible paleoearthquakes were recorded at the Wuzunxiaoer site, and seven suspected events were excluded. Events W1, W2, W3 and W4 exhibit more than one high-quality event indicator (rank 4) sufficient to identify an individual earthquake horizon. The event horizons of units 195, 250, 260, 270, 290, 320 and 350 are excluded due to low-quality event indicators with ranks less than 3, reducing the possibility of overestimating the number of events.

A rupture can be missed during a depositional hiatus, which can be identified from the deposition rate and characteristics of the strata. There are an insufficient number of dating samples from the Wuzunxiaoer trenches to constrain the deposition rate in detail to identify such a hiatus. However, the trenches are located in the central part of the pull-apart basin and are near the source areas. As long as rainfall can form ground runoff, debris can be deposited at the location of the trench. Therefore, there may not be depositional hiatuses in the trenches. In addition, paleosoils were not found in the strata in the trenches, which further indicated that long-term depositional hiatuses do not exist.

The local superimposition of deformation by a younger earthquake on older deformation could hide or obscure evidence of older earthquakes. In trench T4, the indicators for the early events are partially modified by later events (see Section 3.3). Although there is no definitive way to rule out this possibility, complex branch faults, high-resolution strata, high sedimentation rates and multiple exposures can greatly reduce this effect. In T4, the fault zone, which has many branches, is nearly 30 m wide. Moreover, the earthquake evidence on both walls of T4 shows similar features, demonstrating the robustness of the evidence from exposure to exposure. Thus, we conclude that four events likely occurred at the site over past 3500 years.

4.2 Paleoseismic recurrence characteristics and correlation with other sites

The recurrence behavior of paleoearthquakes is crucial for future seismic hazard assessments. Although the ages of the three older events cannot be completely individually distinguished in the Wuzunxiaoer trenches, events W2 and W3 occurred within 200 years (Figure 7), indicating clustered recurrence characteristics. The earliest event (W4) and the most recent event (W1) are separated by ~1000 years from the clustered events. In addition, samples ATF14-22 and ATF14-23 only differ by 200 years, which defines a deposition rate of 7.2 mm yr^{-1}; this is significantly higher than those of the upper and lower strata (Figure 7). Although the ages of the two samples are consistent with their stratigraphic sequence, sample ATF14-23 may be younger considering the overall changes in the deposition rate in the trench. Even so, the older three events (W2, W3 and W4) occurred within ~1000 years, which still indicates clustered characteristics.

To more fully understand the characteristics of the paleoearthquakes along the Wuzunxiaoer section, we compare the data in this study with previously published data (Figure 11; Washburn et al., 2001, 2003; Shao et al., 2018; Yuan et al., 2018). Two events, K1 (AD1230–1720) and K2 (68BC–AD1267), were identified at the Kulesayi site, located ~7 km west of the Wuzunxiaoer site, using radiocarbon and optically stimulated luminescence (OSL) dating methods (Washburn et al., 2001). Both upper boundaries of the latest events at the Kulesayi site were constrained by using the mixed-mineral infrared luminescence method. However, the

Table 1 Dating samples in the Wuzunxiaoer trenches

Sample name	Laboratory number	Unit	^{14}C age	Uncertainty (1σ)	Material	Modeled age (Posterior)
ATF14-06	UCI-153582	50-1	195	15	Animal dung	AD1660–1953
ATF14-04	UCI-153583	50-2	830	20	Animal dung	AD1169–1256
ATF14-22	UCI-153584	155	2180	15	Animal dung	355–174BC
ATF14-23	UCI-153585	195	2355	15	Animal dung	470–389BC
ATF14-17	UCI-153586	205	3230	15	Animal dung	1528–1448BC

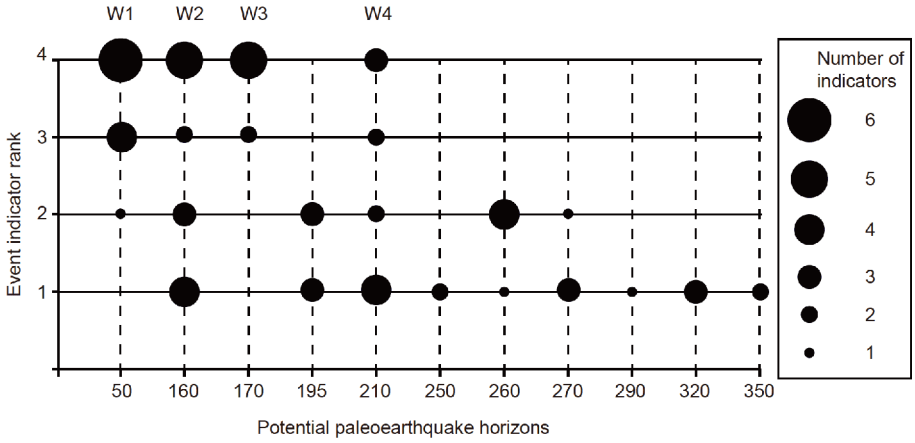

Figure 10 Histograms of event indicators. The diameters of the solid circles are scaled by the sum of the indicators in each rank.

conventional mixed-mineral infrared luminescence signal has abnormal attenuation, which may lead to an underestimation; infrared luminescence signals from fine-grained mixed minerals may have anomalous fading problems that may lead to age overestimation (Wintle, 1973; Huntley and Lamothe, 2001). Therefore, the dating results include these uncertainties, which make it impossible to accurately assess the reliability of the times of the two events. Despite the many uncertainties, we compare the record at the Wuzunxiaoer site to events K1 and K2 at the Kulesayi site. The age range of event W1 strongly overlaps with the date of the most recent event at the Kulesayi site. Considering that continuous surface ruptures span the two sites with no significant steps in map view, it is very likely that W1 ruptured the entire Wuzunxiaoer section. The other event (K2) was not recorded at the Wuzunxiaoer site, indicating that K2 was likely a small earthquake.

In addition to the comparison of the data along the Wuzunxiaoer section, we also compare our results to the data along the Xorkoli section and the Aksay bend (Figure 11). Yuan et al. (2018) discussed the comparison of paleoearthquake records on the Xorkoli section and the Aksay bend. This paper will not repeat the details and focuses on comparing the data on both sides of the Pingdingshan restraining step. Event W1 overlaps in time with the most recent event (A) at the Copper Mine site, so the two events may be the same earthquake. Moreover, the distribution of the coseismic offsets at the Kulesayi site shows that the average strike-slip offset of event W1 is ~6.6 m, suggesting that the magnitude of event W1 may have reached ~M_w7.8 and that the rupture length may have been greater than 200 km (Wells and Coppersmith, 1994). In addition, Elliott et al. (2015) inferred that the magnitude of the latest earthquake was M_w7.8–8.1 based on the latest seismic surface rupture extending continuously from Xorkoli to Annanba. This is consistent with the simultaneous rupture lengths on both sides of the Pingdingshan step, indicating that events W1 and A are the same event not only in time but also in rupture scale. The three other events (W2, W3 and W4) do not correlate with any events at the Copper Mine site, so none of these events passed through the Pingdingshan step. In addition, since 3.5 ka, the Wuzunxiaoer site and the Copper Mine site recorded 4 and 5 events, respectively. In other words, the probabilities of the Wuzunxiaoer section and Xorkoli section participating in cascade failure are 0.25 (1/4) and 0.20 (1/5), respectively, and the Pingdingshan step likely halted most earthquake ruptures.

The angle of the Pingdingshan bend reaches ~25°, and its linking section is ~23 km long. In addition, a ~4 km releasing step is located on the east side of the Pingdingshan bend (Figure 1 and Figure 11). Lozos et al. (2011) show that bends greater than 18° and with linking lengths longer than 5 km usually halt ruptures. In addition, there is a threshold dimension of fault steps (3~4 km) above which earthquake

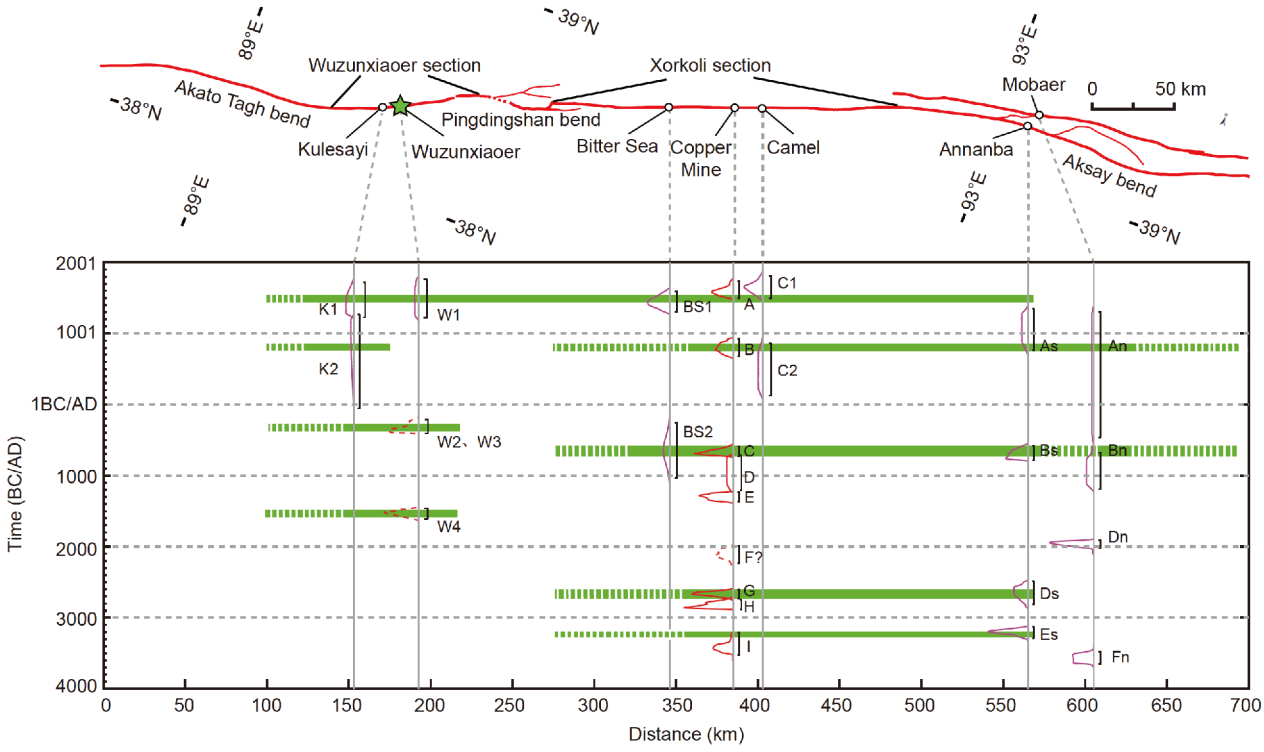

Figure 11 Comparison of the Wuzunxiaoer, Kulesayi, Bitter Sea, Copper Mine, Camel, Annanba and Mobaer rupture records (Washburn et al., 2001, 2003; Yuan et al., 2018; Shao et al., 2018). The solid lines are the PDFs of probable earthquakes, while the dashed lines represent earthquakes with greater uncertainty. The horizontal green bars show the possible rupture extents of paleoearthquakes. The vertical black bars represent the 95% ranges of individual earthquake ages at each site.

ruptures do not propagate and below which rupture propagation ceases only approximately 40% of the time (Wesnousky, 2006). This conclusion is based on numerical simulations of fault ruptures and historical earthquake statistics. However, several strong earthquakes have broken through multiple steps, such as the 1992 Landers earthquake in the USA and the 2016 Kaikōura earthquake in New Zealand (Sieh et al., 1993; Hamling et al., 2017). Although it is impossible to exclude the possibility that two different events that occurred within decades might be considered the same event, the paleoseismic data along the Wuzunxiaoer and Xorkoli sections support the possibility that the most recent earthquake ruptured both sections. In addition to the possibility of simultaneous rupture on both sides of the bend, the occurrence times of the events on the two sections are similar, such as events W4 and E and events W2, W3 and C, indicating that even if the earthquakes cannot break through the Pingdingshan step, there is a relationship between the rupturing times on the two sections.

4.3 Estimation of the sizes of paleoearthquakes

The magnitudes of paleoseismic events can be roughly estimated based on parameters such as the surface rupture length and average coseismic displacement (Wells and Coppersmith, 1994). Estimates of the surface rupture length, coseismic slip and rupture width for the four events at the Wuzunxiaoer site are listed in Table 2. The surface rupture length is estimated based on the comparison of paleoseismic records at multiple sites (Figure 11). The rupture length of event W1 may have reached ~400 km, and W2, W3 and W4 might have reached ~90 km because the Wuzunxiaoer section is confined by a larger-scale bend to the west. Based on these rupture lengths alone, the magnitude of event W1 could have reached M_w8.1, and the other three events could have reached M_w7.3. Because the trench is perpendicular to the fault zone, only the apparent vertical offset of the strata could be obtained. Assuming that the strata are horizontal and that their thicknesses remain constant along the fault between the trench exposures, the average vertical slips of the four paleoseismic events (from new to old) were 0.42, 0.39, 0.11 and 0.48 m, respectively. The coseismic lateral slip of event W1 was 6.6 m, and the ratio of lateral to vertical slip was 15.7. If this ratio is the same for the three older events, the lateral displacements would have been 6.1, 1.7 and 7.6 m for W2, W3 and W4, respectively. Thus, the magnitudes of the four events could have reached M_w7.8, M_w7.7, M_w7.3 and M_w7.8, respectively, based only on the coseismic lateral slips. The widths of the rupture zones of the four events appear to support the scenario that events W1 and W4 were similar in size and larger than events W2 and W3 (see Table 2), assuming that a larger deformation width corresponds to a

Table 2 Estimates of the magnitudes of the four most recent paleoearthquakes at the Wuzunxiaoer site[a)]

Events	FZW	VD (SW wall)	VD (NE wall)	AVD	LD	SRL	M_w (LD)	M_w (SRL)
W1	25	0.47	0.36	0.42	6.6	~400	7.8	8.1
W2	12.5	0.48	0.29	0.39	6.1	~90	7.7	7.3
W3	3	0.08	0.14	0.11	1.7	~90	7.3	7.3
W4	23	0.31	0.65	0.48	7.6	~90	7.8	7.3

a) FZW, fault zone width (m); VD, coseismic vertical displacement (m); AVD, average coseismic vertical displacement (m); LD, coseismic lateral displacement (m); SRL, surface rupture length (km); M_w(LD), moment magnitude based on the empirical relationship between magnitude and average lateral displacement of Wells and Coppersmith (1994); M_w(SRL), moment magnitude based on the empirical relationship between magnitude and surface rupture length.

larger magnitude. However, the magnitudes of the four paleoseismic events are estimated based on several assumptions, and there is great uncertainty in the estimation of the magnitudes, especially for the three older events, which lack reliable lateral displacement data.

5. Conclusions

The small pull-apart basin to the west of Wuzunxiaoer Lake is an ideal site for recording paleoearthquakes because of the high-resolution stratigraphy sourced from two different drainages with different rock types. Four events were identified based on folds, thickened strata, vertical offsets, open fissures, and unconformities. Event W1 occurred between AD1220 and 1773, events W2 and W3 occurred during 407–215BC, and event W4 occurred slightly earlier at 1608–1462BC, suggesting a clustered recurrence behavior. A comparison of the Wuzunxiaoer earthquake record with records at other sites to the east along the Xorkoli section suggests that the most recent earthquake (W1) may have ruptured through the Pingdingshan step-over with a magnitude possibly reaching ~M_w8.1. The older events do not overlap in time but occurred at similar times and may have had smaller magnitudes than the latest event.

Although the Wuzunxiaoer site has high-resolution stratigraphy, materials suitable for carbon dating are sparse, which results in larger uncertainties in the dates of the events than those at sites along the Xorkoli section of the fault. Therefore, additional work is needed at this site, such as excavating more trenches to increase the chances of finding more carbon dating samples and exploiting other dating methods, such as OSL dating.

Acknowledgements *We thank two anonymous reviewers for their constructive reviews that improve the quality and clarity of the work, Wenying Fan for his help in excavating the trenches, and Dr. Alastair Sloan of the University of Cape Town for language editing. This research was supported by National Natural Science Foundation of China (Grant Nos. U1839203, 41761144065, 41802228), Central Public-Interest Scientific Institution Basal Research Fund (Grant No. IGCEA1814), and State Key Laboratory of Earthquake Dynamics of China (Grant No. LED2017A01).*

References

Biasi G P, Wesnousky S G. 2016. Steps and gaps in ground ruptures: Empirical bounds on rupture propagation. Bull Seismol Soc Am, 106: 1110–1124

Biasi G P, Wesnousky S G. 2017. Bends and ends of surface ruptures. Bull Seismol Soc Am, 107: 2543–2560

Chen B L, Cui L L, Bai Y F, Wang S X, Chen Z L, Li X Z, Qi W X, Liu R. 2010. A determining on the displacement of the Altun Tagh sinistral strike-slip fault, NW China: New evidence from the tectonic metallogenetic belt in the eastern part of Altun Tagh Mountain (in Chinese). Acta Petrol Sin, 26: 3387–3396

Chen X H, Yin A, Gehrels E G, Jiang R B, Chen Z L, Bai Y F. 2009. Geothermochronology and tectonic evolution of Eastern Altyn Tagh Mountains, Northwestern China (in Chinese). Earth Sci Front, 16: 207–219

Chen Y, Gilder S, Halim N, Cogné J P, Courtillot V. 2002. New paleomagnetic constraints on central Asian kinematics: Displacement along the Altyn Tagh fault and rotation of the Qaidam Basin. Tectonics, 21: 6-1–6-19

Cheng F, Guo Z, Jenkins H S, Fu S, Cheng X. 2015. Initial rupture and displacement on the Altyn Tagh fault, northern Tibetan Plateau: Constraints based on residual Mesozoic to Cenozoic strata in the western Qaidam Basin. Geosphere, 11: 921–942

Chinese State Bureau of Seismology. 1992. The Altyn Tagh active fault system (in Chinese). Beijing: Seismology Publishing House. 319

Cowgill E, Arrowsmith J R, Yin A, Wang X F, Chen Z L. 2004. The Akato Tagh bend along the Altyn Tagh fault, northwest Tibet 2: Active deformation and the importance of transpression and strain hardening within the Altyn Tagh system. Geol Soc Am Bull, 116: 1443–1464

Cowgill E, Gold R D, Xuanhua C, Xiao-Feng W, Arrowsmith J R, Southon J. 2009. Low Quaternary slip rate reconciles geodetic and geologic rates along the Altyn Tagh fault, northwestern Tibet. Geology, 37: 647–650

Cui J W. 2011. Ductile shearing age of the south Altun fault and its tectonic implications (in Chinese). Acta Petrol Sin, 27: 3422–3434

Ding G Y. 1995. Paleoearthquakes along the Altun active fault and its segmentation (in Chinese). Quat Sci, 15: 97–106

Duan B, Oglesby D D. 2005. Multicycle dynamics of nonplanar strike-slip faults. J Geophys Res, 110: B03304

Elliott A J, Oskin M E, Liu-Zeng J, Shao Y. 2015. Rupture termination at restraining bends: The last great earthquake on the Altyn Tagh fault. Geophys Res Lett, 42: 2164–2170

Elliott A J, Oskin M E, Liu-Zeng J, Shao Y X. 2018. Persistent rupture terminations at a restraining bend from slip rates on the eastern Altyn Tagh fault. Tectonophysics, 733: 57–72

Gao R, Li P W, Li Q S, Guan Y, Shi D N, Kong X R, Liu H B. 2001. Deep process of the collision and deformation on the northern margin of the Tibetan Plateau: Revelation from investigation of the deep seismic profiles. Sci China Ser D-Earth Sci, 44(Suppl): 71–78

Gold R D, Cowgill E, Arrowsmith J R, Chen X, Sharp W D, Cooper K M, Wang X F. 2011. Faulted terrace risers place new constraints on the late Quaternary slip rate for the central Altyn Tagh fault, northwest Tibet.

Geol Soc Am Bull, 123: 958–978
Hamling I J, Hreinsdóttir S, Clark K, Elliott J, Liang C, Fielding E, Litchfield N, Villamor P, Wallace L, Wright T J, D'Anastasio E, Bannister S, Burbidge D, Denys P, Gentle P, Howarth J, Mueller C, Palmer N, Pearson C, Power W, Barnes P, Barrell D J A, Van Dissen R, Langridge R, Little T, Nicol A, Pettinga J, Rowland J, Stirling M. 2017. Complex multifault rupture during the 2016 M_w7.8 Kaikōura earthquake, New Zealand. Science, 356: eaam7194
He J K, Vernant P, Chéry J, Wang W M, Lu S J, Ku W F, Xia W H, Bilham R. 2013. Nailing down the slip rate of the Altyn Tagh fault. Geophys Res Lett, 40: 5382–5386
Huntley D J, Lamothe M. 2001. Ubiquity of anomalous fading in K-feldspars and the measurement and correction for it in optical dating. Can J Earth Sci, 38: 1093–1106
Jiang X D, Yu J, Mcnutt M K. 2004. Lithospheric deformation beneath the Altyn Tagh and West Kunlun faults from recent gravity surveys. J Geophys Res, 109: B05406
Li H B, Xu Z Q, Yang J S, Qi X X, Tapponnier P. 2007. The maximum cumulative strike-slip displacement of the Altyn Tagh fault—900 km (in Chinese)? Geol Bull China, 26: 1288–1298
Li H B, Yang J S, Xu Z Q, Su Z M, Tapponnier P, Van Der Woerd J, Mériaux A S. 2006. The constraint of the Altyn Tagh fault system to the growth and rise of the northern Tibetan plateau (in Chinese). Earth Sci Front, 13: 59–79
Li H B, Yang J S, Xu Z Q, Wu C L, Wan Y S, Shi R D, Liou J G, Tapponnier P, Ireland T R. 2001. Geological and chronological evidence of Indosinian strike-slip movement in the Altyn Tagh fault zone (in Chinese). Chin Sci Bull, 46: 1333–1338
Li K, Xu X W, Luo H, Tapponnier P, Klinger Y, Gao M X. 2016. Paleoseismic events in Banguoba trench along Aksay segment of the Altyn Tagh fault zone (in Chinese). Seismol Geol, 38: 670–679
Li Y C, Shan X J, Qu C Y, Liu Y H, Han N N. 2018. Crustal deformation of the Altyn Tagh fault based on GPS. J Geophys Res-Solid Earth, 123: 10309–10322
Liu J, Xu X W, Li Y F, Ran Y K. 2007. On the completeness of paleoseismic records of strike-slip faults: An example from the Laohushan segment of the Haiyuan fault in Gansu, China, with a discussion of several problems in the paleoearthquake study (in Chinese). Geol Bull China, 26: 250–260
Liu Y J, Neubauer F, Ge X H, Genser J, Yuan S H, Li W M, Gong Q L, Chen Y Z. 2007. Geochronology of the Altun fault zone and rising of the Altun Mountains (in Chinese). Chin J Geol, 42: 134–146
Lozos J C, Oglesby D D, Duan B, Wesnousky S G. 2011. The Effects of double fault bends on rupture propagation: A geometrical parameter study. Bull Seismol Soc Am, 101: 385–398
Mériaux A S, Tapponnier P, Ryerson F J, Xiwei X, King G, Van der Woerd J, Finkel R C, Haibing L, Caffee M W, Zhiqin X, Wenbin C. 2005. The Aksay segment of the northern Altyn Tagh fault: Tectonic geomorphology, landscape evolution, and Holocene slip rate. J Geophys Res, 110: B04404
Mériaux A S, Van der Woerd J, Tapponnier P, Ryerson F J, Finkel R C, Lasserre C, Xu X W. 2012. The Pingding segment of the Altyn Tagh fault (91°E): Holocene slip-rate determination from cosmogenic radionuclide dating of offset fluvial terraces. J Geophys Res, 117: B09406
Molnar P, Burchfiel B C, K'uangyi L, Ziyun Z. 1987. Geomorphic evidence for active faulting in the Altyn Tagh and northern Tibet and qualitative estimates of its contribution to the convergence of India and Eurasia. Geology, 15: 249–253
Molnar P, Tapponnier P. 1975. Cenozoic Tectonics of Asia: Effects of a Continental Collision: Features of recent continental tectonics in Asia can be interpreted as results of the India-Eurasia collision. Science, 189: 419–426
Peltzer G, Tapponnier P, Armijo R. 1989. Magnitude of late Quaternary left-lateral displacements along the north edge of Tibet. Science, 246: 1285–1289
Ramsey C B, Lee S. 2013. Recent and planned developments of the program OxCal. Radiocarbon, 55: 720–730
Ran Y K, Wang H, Li Y B, Chen L C. 2012. Key techniques and several cases analysis in paleoseismic studies in mainland China (1): Trenching sites, layouts and paleoseismic indicators on active strike-slip faults (in Chinese). Seismol Geol, 34: 197–210
Reimer P J, Bard E, Bayliss A, Beck J W, Blackwell P G, Ramsey C B, Buck C E, Cheng H, Edwards R L, Friedrich M, Grootes P M, Guilderson T P, Haflidason H, Hajdas I, Hatté C, Heaton T J, Hoffmann D L, Hogg A G, Hughen K A, Kaiser K F, Kromer B, Manning S W, Niu M, Reimer R W, Richards D A, Scott E M, Southon J R, Staff R A, Turney C S M, van der Plicht J. 2013. IntCal13 and Marine13 radiocarbon age calibration curves 0–50000 years cal BP. Radiocarbon, 55: 1869–1887
Ritts B D, Biffi U. 2000. Magnitude of post-Middle Jurassic (Bajocian) displacement on the central Altyn Tagh fault system, northwest China. Geol Soc Am Bull, 112: 61–74
Scharer K M, Weldon R J, Fumal T E, Biasi G P. 2007. Paleoearthquakes on the Southern San Andreas Fault, Wrightwood, California, 3000 to 1500 BC: A new method for evaluating paleoseismic evidence and earthquake horizons. Bull Seismol Soc Am, 97: 1054–1093
Shao Y X, Liu-Zeng J, Oskin M E, Elliott A J, Wang P, Zhang J Y, Yuan Z D, Li Z G. 2018. Paleoseismic investigation of the Aksay restraining double bend, Altyn Tagh Fault, and its implication for barrier-Breaching ruptures. J Geophys Res-Solid Earth, 123: 4307–4330
Sieh K, Jones L, Hauksson E, Hudnut K, Eberhart-Phillips D, Heaton T, Hough S, Hutton K, Kanamori H, Lilje A, Lindvall S, McGill S F, Mori J, Rubin C, Spotila J A, Stock J, Kie Thio H, Treiman J, Wernicke B, Zachariasen J. 1993. Near-field investigations of the Landers earthquake sequence, April to July 1992. Science, 260: 171–176
Sobel E R, Arnaud N. 1999. A possible middle Paleozoic suture in the Altyn Tagh, NW China. Tectonics, 18: 64–74
Sun Z M, Li H B, Pei J L, Xu W, Pan J W, Si J L, Zhao L S, Zhao Y. 2012. Strike-slip movement of theAltyn Tagh fault and implications for mountain formation inferred from paleomagnetic data in northeastern Tibetan Plateau (in Chinese). Acta Petrol Sin, 28: 1928–1936
Tapponnier P, Zhiqin X, Roger F, Meyer B, Arnaud N, Wittlinger G, Jingsui Y. 2001. Oblique stepwise rise and growth of the Tibet plateau. Science, 294: 1671–1677
Wang E. 1997. Displacement and timing along the northern strand of the Altyn Tagh fault zone, Northern Tibet. Earth Planet Sci Lett, 150: 55–64
Wang F, Xu X W, Zheng R Z, Chen W B. 2004. Late Quaternary slip-rate on the Altun fault west to the Qarqan River (in Chinese). Seismol Geol, 26: 200–208
Washburn Z, Arrowsmith J R, Dupont-Nivet G, Wang X F, Zhang Y, Chen Z L. 2003. Paleoseismology of the Xorxol segment of the central Altyn Tagh fault, Xinjiang, China (in Chinese). Ann Geophys, 46: 1015–1034
Washburn Z, Arrowsmith J R, Forman S L, Cowgill E, Wang X F, Zhang Y, Chen Z L. 2001. Late Holocene earthquake history of the central Altyn Tagh fault, China. Geology, 29: 1051–1054
Wells D L, Coppersmith K J. 1994. New empirical relationships among magnitude, rupture length, rupture width, rupture area, and surface displacement (in Chinese). Bull Seismol Soc Am, 84: 974–1002
Wesnousky S G. 2006. Predicting the endpoints of earthquake ruptures. Nature, 444: 358–360
Wintle A G. 1973. Anomalous fading of thermo-luminescence in mineral samples. Nature, 245: 143–144
Wittlinger G, Tapponnier P, Poupinet G, Mei J, Danian S, Herquel G, Masson F. 1998. Tomographic evidence for localized lithospheric shear along the Altyn Tagh fault. Science, 282: 74–76
Wu L, Gong Q L, Qin S H. 2013. When did Cenozoic left-slip along the Altyn Tagh Fault initiate? A comprehensive approach (in Chinese). Acta Petrol Sin, 29: 2837–2850
Wu L, Xiao A C, Wang L Q, Mao L G, Wang L, Dong Y P, Xu B. 2012. EW-trending uplifts along the southern side of the central segment of the Altyn Tagh Fault, NW China: Insight into the rising mechanism of the Altyn Mountain during the Cenozoic. Sci China Earth Sci, 55: 926–939

Xiao Q, Yu G, Liu-Zeng J, Oskin M E, Shao G H. 2017. Structure and geometry of the Aksay restraining double bend along the Altyn Tagh fault, Northern Tibet, imaged using magnetotelluric method. Geophys Res Lett, 44: 4090–4097

Xu X W, Wang F, Zheng R Z, Chen W B, Ma W T, Yu G H, Chen G H. 2005. Late Quaternary sinistral slip rate along the Altyn Tagh. Sci Chin Ser D-Earth Sci, 48: 384

Xu X W, Yu G H, Chen G H, Li C X, Zhang L F, Klinger Y, Tapponnier P, Liu J. 2007. Near-surface character of permanent geologic deformation across the mega-strike-slip faults in the northern Tibetan Plateau (in Chinese). Seismol Geol, 29: 201–217

Xu Z Q, Li H B, Tang Z M, Qi X X, Li H Q, Cai Z H. 2011. The transformation of the terrain structures of the Tibet Plateau through large-scale strike-slip faults (in Chinese). Acta Petrol Sin, 27: 3157–3170

Yin A, Rumelhart P E, Butler R, Cowgill E, Harrison T M, Foster D A, Ingersoll R V, Zhang Q, Zhou X Q, Wang X F, Hanson A, Raza A. 2002. Tectonic history of the Altyn Tagh fault system in northern Tibet inferred from Cenozoic sedimentation. Geol Soc Am Bull, 114: 1257–1295

Yuan Z D, Liu J, Li Z F, Shao Y X, Li Z G, Wang P, Wang W, Yao W Q. 2016. Tecto-geomorphic analysis of paleoseismic trenching sites on active strike-slip faults (in Chinese). Geol Bull China, 35: 1807–1828

Yuan Z D, Liu-Zeng J, Wang W, Weldon R J, Oskin M E, Shao Y X, Li Z G, Wang P, Zhang J Y. 2018. A 6000-year-long paleoseismologic record of earthquakes along the Xorkoli section of the Altyn Tagh fault, China. Earth Planet Sci Lett, 497: 193–203

Yuan Z D. 2018. Long Paleoseismic record on the Wuzunxiaoer-Xorkoli section of the central Altyn Tagh fault (in Chinese). Doctoral Dissertation. Beijing: Institute of geology, China Earthquake Administration

Yue Y J, Liou J G. 1999. Two-stage evolution model for the Altyn Tagh fault, China. Geology, 27: 227–230

Zhang L T, Unsworth M, Jin S, Wei W B, Ye G F, Jones A G, Jing J E, Dong H, Xie C L, Pape F L, Vozar J. 2015. Structure of the Central Altyn Tagh Fault revealed by magnetotelluric data: New insights into the structure of the northern margin of the India-Asia collision. Earth Planet Sci Lett, 415: 67–79

Zhang P Z, Molnar P, Xu X. 2007. Late Quaternary and present-day rates of slip along the Altyn Tagh Fault, northern margin of the Tibetan Plateau. Tectonics, 26: TC5010

Zhao J M, Mooney W D, Zhang X K, Li Z C, Jin Z J, Okaya N. 2006. Crustal structure across the Altyn Tagh Range at the northern margin of the Tibetan Plateau and tectonic implications. Earth Planet Sci Lett, 241: 804–814

(Responsible editor: Maoyan ZHU)